1   **Crude oil cardiotoxicity to red drum embryos is independent of oil dispersion energy**

2   Jeffrey M. Morris[1], Michel Gielazyn[2], Michelle O. Krasnec[1], Ryan Takeshita[1], Heather P. Forth[1],

3   Jana S. Labenia[3], Tiffany L. Linbo[3], Barbara L. French[3], J. Anthony Gill[3], David H. Baldwin[3],

4   Nathaniel L. Scholz[3], and John P. Incardona[3]*

5   [1]Abt Associates, 1881 Ninth St., Suite 201, Boulder, Colorado, 80302

6   [2]National Oceanic and Atmospheric Administration, Assessment and Restoration Division, 263

7   13th Ave. South, St. Petersburg, Florida, 33701

8   [3] Environmental and Fisheries Science Division, Northwest Fisheries Science Center, National

9   Marine Fisheries Service, National Oceanic and Atmospheric Administration, 2725 Montlake

10   Blvd. E., Seattle, Washington, 98112

11

12

13   *Corresponding author: John P. Incardona
14   NOAA Fisheries
15   Northwest Fisheries Science Center
16   2725 Montlake Blvd. E.
17   Seattle, WA 98112
18   Voice: (206) 860 –
19   Fax: (206) 860-3335
20   Email: John.Incardona@noaa.gov
21
22

Abstract

The potential bioavailability of toxic chemicals from oil spills to water column organisms such as fish embryos may be influenced by physical dispersion along an energy gradient. For example, a surface slick with minimal wave action (low energy) could potentially produce different toxic effects from high energy situations such as pressurized discharge from a blown wellhead. Here we directly compared water accommodated fractions (WAFs) of oil prepared with low and high mixing energy (LEWAFs and HEWAFs, respectively) using surface oil samples collected during the 2010 *Deepwater Horizon* spill, and exposing embryos of a representative nearshore species, red drum (*Sciaenops ocellatus*). Biological effects of each WAF type was quantified with several functional and morphological indices of developmental cardiotoxicity, providing additional insight into species-specific responses to oil exposure. Although the two WAF preparations yielded different profiles of polycyclic aromatic hydrocarbons (PAHs), some cardiotoxic phenotypes were very similar. Based on benchmark thresholds for both morphological and functional cardiotoxicity, in general LEWAFs had lower thresholds than HEWAFs based on total PAH measures. However, HEWAF and LEWAF toxicity thresholds were more similar when calculated based on estimates of dissolved PAHs only.

Highlights

- Low and high energy water accommodated fractions of crude oil were compared

- Toxic effects were assessed using cardiotoxicity endpoints in red drum embryos

- The biological effects of both WAF types were virtually identical

- Differences in toxic threshold levels based on ∑PAH measures were observed

1. Introduction

49   The *Deepwater Horizon* (DWH) oil spill began on April 20, 2010. The damaged

50   wellhead on the Northern Gulf of Mexico (GoM) seafloor subsequently released millions of

51   barrels of crude oil into the ocean until the well was eventually capped on July 15, 2010 (Camilli

52   et al., 2010; The Federal Interagency Solutions Group, 2010). The event was the largest marine

53   oil spill in U.S. history. The spill was also unusual in that it originated in the deep ocean, under

54   extreme pressure, with chemical dispersants used at both the wellhead and on the ocean surface.

55   The result was chemically and mechanically dispersed petroleum compounds, including

56   polycyclic aromatic hydrocarbons (PAHs), in a wide range of GoM environments that are

57   essential for commercially and recreationally important fisheries (Ylitalo et al., 2012). Many

58   species of fish were spawning during the active spill phase, or in the months after capping, in

59   both nearshore and offshore nursery habitats.

60   The impacts of crude oil on fish early life stages are now fairly well known (Incardona et

61   al., 2009; McIntosh et al., 2010; Dubansky et al., 2013; Incardona et al., 2014; Mu et al., 2014;

62   Jung et al., 2015; Madison et al., 2015). This focal line of research largely began in the

63   aftermath of the 1989 Exxon Valdez oil spill, which extensively oiled coastal streams and

64   shoreline spawning areas for pink salmon and Pacific herring, respectively, in Prince William

65   Sound, Alaska (Peterson et al., 2003). Crude oil exposures cause a familiar syndrome of

66   developmental defects in virtually all fish species tested, including fluid accumulation (edema) in

67   the vicinity of the heart or the yolk sac, as well as craniofacial and body axis abnormalities

68   (Incardona and Scholz, 2016). Mechanistic studies in zebrafish, an experimental model for

69   development toxicity in fish and humans, revealed the heart to be the primary target organ for

70   crude-oil derived PAHs, with visible extracardiac defects arising as secondary sequelae

71   (Incardona and Scholz, 2016; Incardona, 2017). Certain PAHs – particularly those having three

72 rings (tricyclics) – disrupt heart muscle cell repolarization and calcium cycling (Brette et al.,

73 2014; Brette et al., 2017). This in turn disrupts the normal rhythm and contractility of the

74 embryonic heart (Incardona et al., 2009; Jung et al., 2013; Incardona et al., 2014; Sørhus et al.,

75 2016). Cardiac morphogenesis depends on a functional heart, and perturbations in rhythm or

76 output can lead to permanent and adverse changes in heart shape at later life stages (Hicken et

77 al., 2011; Incardona et al., 2015; Incardona, 2017). Thus, relatively low crude oil exposure

78 concentrations cause the developing heart to fail, leading to severe downstream anatomical

79 defects and larval death.   Fish may survive transient exposures to oil at even lower (trace)

80 concentrations, but consequent changes in cardiac morphogenesis can cause lasting changes in

81 heart shape that correspond to impaired swimming performance (Hicken et al., 2011; Incardona

82 et al., 2015).

83 Whereas the majority of older studies focused on cold-water species impacted by the

84 Exxon Valdez spill, the DWH disaster led to an expanded focus on a wider variety of species

85 representing distinct ecophysiological niches. First, oil from the DWH-Macondo 252 (MC252)

86 well has proven to be relatively conventional in terms of toxicity to fish early life stages. Crude

87 oils from the MC252 well and the Alaska North Slope (Exxon Valdez) produced nearly identical

88 injury phenotypes in zebrafish embryos and larvae (Incardona et al., 2013). However, studies on

89 MC252 crude oil-induced cardiotoxicity in the early life stages of large pelagic predators such as

90 bluefin (*Thunnus maccoyii*) and yellowfin tuna (*Thunnus albacares*) (Incardona et al., 2014), as

91 well as mahi mahi (*Coryphaena hippurus*) (Edmunds et al., 2015; Esbaugh et al., 2016)

92 demonstrated species-specific variation attributable to differences in developmental anatomy and

93 ecophysiology (Incardona and Scholz, 2016). For those studies, a simple and readily

94 reproducible method for producing high energy dispersions of oil droplets in the water column

4

95   (high energy water-accommodated fractions, or HEWAFs: (Incardona et al., 2013)) was

96   developed to mimic exposure conditions that might have existed for open ocean pelagic species

97   spawning in the vicinity of the damaged wellhead, where plumes of small oil droplets rose to the

98   surface.

99   In addition to contaminating pelagic fish spawning habitats in the northern GoM, MC252

100 crude also came ashore (Nixon et al., 2016), thereby oiling embayments and marsh nursery

101 habitats for red drum (*Sciaenops ocellatus*), speckled sea trout, and other economically important

102 species that spawn in shallow coastal waters (Lowerre-Barbieri et al., 2016). Whereas visible oil

103 disappeared in the upper surface waters of the pelagic zone relatively soon after the wellhead

104 was capped, oil persisted in some shoreline habitats for up to two years (Michel et al., 2013).

105 Besides impacts on fish actively spawning in the open ocean during the spill, this also suggests

106 the possibility of lingering injury to early life stages of fish species such as red drum that spawn

107 nearshore later in the year (i.e., late summer to early fall). However, the pathway for oil

108 exposure for species such as red drum would have involved lower energy mixing of surface

109 slicks or oil stranded on marsh substrates.

110 Previous studies examined the effects of weathered MC252 oil on red drum embryos

111 (Khursigara et al., 2017; Xu et al., 2017). While those studies used MC252 oil collected from

112 surface slicks, exposures utilized HEWAFs, which are more representative of open ocean

113 habitats closer to the wellhead rather than nearshore areas where red drum actually spawn. At the

114 same time, some investigators have questioned the validity and environmental relevance of these

115 simple HEWAF preparations (Echols et al., 2016; Sandoval et al., 2017). Thus, the primary

116 objective of this study was to directly compare the toxic effects of standard HEWAF

117 preparations to a low energy mixing method that has become an industry standard (Singer et al.,

118 2000). In addition, we provide a more detailed analysis of red drum heart development and

119 cardiotoxic effects that provide additional insight into how the ecophysiology of different fish

120 species determines the precise responses to crude oil exposure during organogenesis.

121 **2. Materials and Methods**

122   This study was conducted in support of the DWH Natural Resource Damage Assessment

123 (NRDA). Detailed descriptions of the protocols and procedures developed and implemented for

124 the NRDA, including the methods used in the current study, are provided elsewhere (Morris et

125 al., 2015).

126 *2.1. Facilities*

127   Red drum husbandry and crude oil exposures were implemented in collaboration with the

128 Texas Parks and Wildlife Department's Sea Center Texas marine hatchery in Lake Jackson, TX.

129 The Sea Center uses filtered water from Galveston Bay as a source of natural seawater. The

130 water for our experiments was obtained directly from the distribution lines for the Sea Center

131 hatchery. Clean (control) seawater was stored in a 340-L carboy covered in dark plastic and

132 maintained under aeration at ambient temperature. Samples were routinely collected from this

133 carboy and analyzed for conventional water quality parameters (e.g., dissolved oxygen, pH,

134 salinity) as well as background contamination (e.g., hydrocarbons, volatile organic compounds,

135 pesticides, metals, major cations and anions, suspended and dissolved solids, turbidity, organic

136 carbon, and chemical and biologic oxygen demand; Table S1). We also collected baseline

137 (control) water samples at the beginning of each exposure. Analytical chemistry was conducted

138 by ALS Environmental (Kelso, WA).

2.2. Red drum

The Sea Center maintains a broodstock of red drum under controlled temperature and diel lighting conditions. The adult fish spawn volitionally in the evening, at which time newly fertilized embryos were removed from egg collector troughs on the spawning tanks. For each spawning event, we visually assessed fertilization success by microscopy for a small subset of embryos. If the spawning event resulted in successful fertilization (>90%), we immediately loaded embryos into beakers containing different exposure solutions. The embryos were not treated with antibiotics in accordance with the conventional husbandry practices at the Sea Center. Animal care and experimental design were carried out with adherence to policy of the U.S. Department of Commerce and Public Health Service, conforming to the standards of the National Academy of Sciences' *Guide for the Care and Use of Laboratory Animals* (Council, 2011).

2.3. Water-accommodated fraction preparation

We used two different MC252 oil samples (Slick A and Slick B) that were collected from the GoM ocean surface during the active phase of the DWH spill. The Slick A sample was collected on July 29, 2010 from the hold of barge number CTC02404, a repository for oil recovered by various skimming vessels responding to the spill. Slick B oil was collected on July 19, 2010 from the U.S. Coast Guard skimmer *Juniper*. The degree of weathering for the Slick A and Slick B samples, as measured by the loss of TPAH51 (TPAH50 listed in Table S2 plus perylene) relative to hopane, was 68% and 85%, respectively (Forth et al., 2017b). We used both oil samples to prepare WAFs using a low-energy (LEWAF) or high-energy (HEWAF) mixing

161   procedure. These exposure methods were standardized for use in parallel NRDA assays on a

162   diversity of GoM species. Briefly, LEWAF solutions were prepared by adding 1 g oil/L

163   seawater to an aspirator bottle (covered) and slowly mixing (no vortex) the solution using a

164   magnetic stirrer for 18-24 hours. After mixing, the LEWAF solution was drained from the

165   bottom of the aspirator bottle, leaving the top layer of settled oil undisturbed. This solution was

166   diluted with clean sea water to achieve target exposure solutions. HEWAF solutions were

167   prepared by adding 1 g oil/L seawater to a commercial stainless steel food blender (Waring

168   CB15), followed by mixing on the low speed setting for 30 seconds. After mixing, the entire

169   solution was poured into a separatory funnel and allowed to settle for 1 hour. After settling, the

170   HEWAF was drained out of the bottom of the funnel, leaving the top layer of settled oil

171   undisturbed. This solution was also diluted with clean sea water to achieve target exposure

172   solutions. The chemical and physical characteristics of the two oil samples, the WAF mixing

173   procedures, and the chemistry profiles of the resulting LEWAF and HEWAF are detailed in

174   publications describing comprehensive WAF characterization studies in support of the DWH

175   NRDA toxicity testing program (Forth et al., 2017a and b).

176   *2.4. Exposures*

177   Two stock WAFs (a LEWAF and a HEWAF) for each oil type were prepared and then

178   diluted in clean seawater to obtain target exposure concentrations by adding different volumes of

179   stock WAF to clean seawater for each exposure concentration. These stock WAFs were diluted

180   nominally to obtain final percent WAF concentrations as follows: Slick A and Slick B LEWAFs:

181   0 (control), 6.25, 12, 25, 50 and 100%; Slick A HEWAF: 0 (control), 0.04, 0.1, 0.24, 0.6, and

182   2%; Slick B HEWAF: 0 (control), 0.4, 1, 2.4, 6, and 15%. Each treatment category (Slick A

183   LEWAF, Slick A HEWAF, Slick B LEWAF, Slick B HEWAF) consisted of five oil

184   concentrations and one control. Diluted WAF stock solution (400 mL) was added into one of

185   four replicate 600-ml glass beakers for each treatment. In addition, a subsample was collected

186   from each dilution for chemical analysis at the onset of each bioassay. Subsequently, 200 newly-

187   fertilized red drum embryos were added to each exposure beaker, a standard density for

188   incubation to hatch in beakers for this species (Holt et al., 1981; Douillet and Pickering, 1999).

189   An additional goal of these experiments was to simultaneously expose sufficient numbers of

190   embryos to produce samples for live imaging, mRNA extraction, and whole-mount in situ

191   hybridization studies. The latter two types of samples necessitate 100+ embryos per replicate,

192   and are the subject of studies to be described elsewhere. Range-finding experiments showed no

193   significant adverse effect of these incubation densities, with average mortality at $21 \pm 9\%$ (s.d.)

194   at 48 hours post fertilization over nine independent assays (raw data available at

195   https://www.diver.orr.noaa.gov/web/guest/dwh-toxicity-studies; test IDs 636-639). At 36 h post

196   fertilization (12 h post-hatch) the mean standard length of beaker-incubated control larvae was

197   2.70 ± 0.03 mm, while the mean length of larvae from hatchery tanks was 2.82 ± 0.03 mm (N =

198   3 each; $p = 0.06$). There was no difference in heart rate between beaker and hatchery incubated

199   controls (185 ± 6 and 194 ± 7 beats/min for two beakers vs. 197 ± 7 and 199 ± 4 beats/min for

200   two hatchery tanks; N = 8 – 17 larvae, ANOVA p = 0.3). Exposure beakers were placed in a

201   water bath (28 °C) for temperature control. Water quality parameters (pH, dissolved oxygen,

202   total ammonia and temperature) were monitored at the beginning and end of each 36-h static

203   bioassay. At 28 °C, red drum typically hatch at ~ 24-h post-fertilization. We determined that

204   optimal visualization of the heart was obtained at 12 h post-hatch. Consequently, after 36 h a

205   subset of hatched (surviving) larvae was removed from each beaker and imaged using

206   videomicroscopy (further details below). All animals were collected from the exposures. The

207   remaining larvae were collected by gently pouring exposure media through nylon mesh cell

208   strainers (Falcon VWR), then microscopically inspected and transferred to tubes for flash

209   freezing in liquid nitrogen or fixation in paraformaldehyde. These samples were retained for

210   other aspects of the study and are otherwise not described here further.

211   *2.5. Image collection and analysis*

212   To collect videos from 30 individual larvae from each replicate in as short a time span as

213   possible, four microscope stations were operated simultaneously. Beakers were randomly

214   selected from the water bath by separate staff and delivered to the microscopy teams. Two or

215   three larvae at a time were randomly captured from each replicate beaker using a wide-bore glass

216   pipette and mounted on a microscope slide in 2% methyl cellulose in clean seawater. Fish were

217   oriented to provide a left-lateral perspective. Digital still images and videos of the entire fish

218   were obtained using a Nikon SMZ800 stereo microscope fitted with a phototube and a Unibrain

219   Fire-i400 1394 camera connected via firewire to a laptop computer with BTV Pro

220   (Bensoftware.com). A 10 second video was recorded for each fish at the highest magnification

221   (6.3x), focusing on the cardiac/pericardial region. Subsequently, still frames of entire larvae

222   selected at random were collected at 2x magnification, as the basis for representative composite

223   images. The above process was repeated until microscopy data were obtained for 30 larvae

224   (15% of the total) from each replicate beaker, for an overall total of 720 larvae from each

225   exposure over a period of 6 hours.

226   Still images and video were analyzed using ImageJ software (https://imagej.nih.gov/ij/).

227   Quantified metrics included atrial and ventricular contraction, atrioventricular (AV) angle, and

228   edema – the latter as pericardial fluid accumulation as well as the volume of the abdomen and

229   yolk sac areas as a whole. Fractional shortening (contractility) was measured for both chambers

230   by drawing a line between the outer edges of the myocardium and perpendicular to the long axis

231   of the chamber at both systole and diastole. This was repeated in triplicate and averaged for each

232   larva, with fractional shortening calculated as (diastolic-systolic)/diastolic * 100). For the same

233   individual, the video was then advanced to the point where the atrium was just beginning to

234   contract and reversed one frame. AV angle was measured on this frame by (1) drawing a line

235   from the outer dorsal edge of the heart where the ventricle and bulbus arteriosus meet (at the

236   location of the AV node); (2) continuing the second segment of this line to the outer dorsal edge

237   of the heart where the atrium and sinus venosus meet; and (3) using the analyze option in ImageJ

238   to report the ensuing angle (Fig. S2). This was repeated in triplicate to obtain a mean value. We

239   measured pericardial area as previously defined (Incardona and Scholz, 2016) by outlining the

240   pericardial sac in ImageJ and using the analyze tool to determine total area. Lastly, thickness of

241   the cardiac jelly was measured in the atrial chambers from frames in which the chamber was in

242   systole, using the line tool in ImageJ to measure the distance between the endocardium and

243   myocardium perpendicular to the long axis of the chamber (Fig. S9).

244   *2.6. Hydrocarbon analysis*

245   250-ml water samples were collected in glass amber bottles from each of the diluted

246   stock solutions (corresponding to each exposure) and shipped overnight on ice to ALS

247   Environmental (Kelso, WA) for hydrocarbon analysis. The samples were solvent-extracted

248   within seven days of collection. Target analytes included PAHs, alkyl PAH homologues, and

249   related hetero-compounds, as determined by gas chromatography using low-resolution mass

250   spectrometry with selected ion monitoring (GC/MS-SIM), in accordance with the U.S.

251   Environmental Protection Agency Method 8270D. Herein, we report total PAH concentrations

252   as the sum of 50 analytes (TPAH50; Table S2) (Forth et al., 2015; Forth et al., 2017b). Using the

253   results of these total hydrocarbon analyses, we then utilized a regression-based modeling

254   approach we have previously applied (Esbaugh et al., 2016; Forth et al., 2017a) to estimate the

255   concentrations of dissolved PAHs in the WAF solutions. Briefly, this included generating

256   regression-based models with empirical data on total and dissolved (filtered) individual PAH

257   concentrations from several different WAF preparations and concentrations (described in detail

258   in Esbaugh et al., 2016).

259   *2.7. Statistical Analysis*

260   Nonlinear curve fits of atrial and ventricular contraction, AV angle, pericardial area, and

261   cardiac jelly thickness versus the log of TPAH50 concentration were performed using a four-

262   parameter logistic equation ($Y = Bottom + (Top - Bottom)/(1 + 10^{((LogEC50 - X) * HillSlope)})$) in

263   Prism 7 (GraphPad Software Inc.). Pericardial area was normalized to controls for each test to

264   account for absolute differences between the controls. To estimate $EC_{20}s$ and benchmark

265   concentrations (BMC) using regressions, the LogEC50 term was modified to fit for an effect

266   level other than 50% (i.e., 20% effect or the benchmark response (BMR), respectively). An

267   upper asymptote bound of the response was estimated for each endpoint separately, using a

268   similar curve-fitting process. The BMC represents the concentration that produces the BMR. For

269   each measurement, the BMR was based on the 5% or 95% quantile of the control measurements

270   (e.g., (Hecht et al., 2007). The confidence intervals for the estimate of EC_{50}, EC_{20}, or BMC were

271   calculated in Prism 7 using the profile likelihood method.

3. Results and Discussion

3.1. Exposure conditions

Mean water quality parameters for the beginning and end of the four bioassays are listed in Table S3. Consistent with the expected presence and absence of whole oil droplets in HEWAFs and LEWAFs, respectively, the two types of preparations resulted in distinctly different PAH compositions in water (Figs. 1 and 2; absolute concentrations shown in Fig. S1). Slick A and B oil samples (Figs. 1A and 2A, respectively) were both relatively heavily weathered, as indicated by the low percentages of naphthalenes. Slick B was very highly weathered, with reduction of naphthalenes to less than 4% from roughly 55% in fresh MC252 source oil (Incardona et al., 2013). The PAH composition of LEWAFs reflected primarily soluble PAHs, with ring-number families dominated by the more water soluble parent compounds, followed by decreasing levels of the less soluble alkylated homologs (Slick A, Fig. 1B and Fig. S1A; Slick B, Fig. 2B and Fig. S1B), consistent with the lack of droplets previously reported for these preparations (Forth et al., 2017a). In contrast, HEWAF preparations of both oils produced waterborne total (dissolved + particulate) PAH compositions that closely matched the whole oils (Slick A, Fig. 1C and Fig. S1C; Slick B, Fig. 2C and Fig. S1D). The exposure concentrations (TPAH50; Table 1) ranged from 1.0 to 31.5 µg/L for Slick A HEWAF, 1.2 to 51.8 µg/L for Slick B HEWAF, 1.0 to 17.9 µg/L for Slick A LEWAF, and 0.04 to 14.8 µg/L for Slick B LEWAF. Because HEWAF measured concentrations included both particulate oil droplets and dissolved PAHs (Table 1), we utilized a previously applied modeling approach (Esbaugh et al., 2016; Forth et al., 2017b) to estimate the concentrations of dissolved PAHs in HEWAFs. These dissolved TPAH50 estimates ranged from 0.6 to 10.1 µg/L for Slick A HEWAF and 0.5 to 4.9 µg/L for Slick B HEWAF (Table 1).

13

295   *3.2. Morphological and functional effects of exposure*

296   Although we visually examined exposed red drum shortly after hatch, our quantitative

297   analyses focused on yolk sac larvae roughly 12-h post-hatch (hph). By this point in

298   development, a large portion of the yolk had been absorbed and the heart was more readily

299   imaged. Control red drum larvae (Fig. 3A) had the typical appearance of pelagic (i.e., floating)

300   marine larvae, with large marginal finfolds, unpigmented eyes, a series of six lateral line

301   neuromasts along the trunk, and a rudimentary gut. Yolk absorption had progressed to the point

302   where there was a small, nearly spherical yolk mass surrounding the yolk oil droplet. Larvae

303   exposed to each WAF and oil type showed a common set of phenotypic characteristics that were

304   grossly indistinguishable (Fig. 3B-3E). Edema accumulated anterior to the yolk mass, typically

305   forcing it posteriorly into a concave shape. In addition, larvae exposed to the upper end of the

306   concentration range tended to have smaller heads and eyes, an effect more apparent from a dorsal

307   perspective (e.g., Fig. 3B, bottom). Although not quantified, exposed larvae also appeared to

308   have reduced subdermal space, evident as scalloping of the dorsal-anterior portion of the finfold

309   in lateral views, and narrower mid-trunk regions in dorsal views. This suggests that fluid

310   accumulation in the yolk sac is due to an internal shift of water from the dorsal and lateral

311   subdermal spaces, as reported for other fish species (Incardona and Scholz, 2016).

312   In addition to edema, exposure to each WAF led to common but specific defects in

313   cardiac function and morphogenesis. In unexposed 12-hph larvae, the transparent yolk mass

314   extended anteriorly all the way to the head, with the heart visible in ventral views between the

315   yolk and branchial arches (Fig. 4A). At this point where the looping of the atrial and ventricular

316   chambers was just beginning, the heart was oriented laterally with the opening of the atrium on

317   the left side. In oil-exposed red drum, edema was evident in the anterior yolk sac by this stage

14

318   (Fig. 4B). By 12-hph the heart was visible in lateral views, and looping had progressed to bring

319   the atrium closer to the midline. At this point there was a sharp angle between the atrium and

320   ventricle in control larvae, with the latter possessing a rough "s" shape (Fig. 4C). Control larvae

321   also had a fairly large pericardial space, with a yolk sinus/pericardial membrane contiguous with

322   the sinus venosus, closely apposed to the remaining yolk mass (Fig. 4C). Exposure to the

323   HEWAFs and LEWAFs of both oil samples led to severe cardiac malformation and marked

324   edema at the higher concentrations (e.g., Slick A HEWAF, Fig. 4D; Slick B LEWAF, Fig. 4E).

325   Cardiac chambers were reduced in size and un-looped in a nearly linear anterior-posterior

326   arrangement, although the atrioventricular junction remained distinguishable in videos (arrows,

327   Fig. 4D, 4E; Movie S1). Edema accumulated in both the pericardial space and the yolk sac

328   sinus, revealing the pericardial/yolk sinus membranes (arrowheads, Fig. 4D, 4E).

329   We determined the magnitude of fluid accumulation, as well as cardiac looping

330   abnormalities, the latter quantified as deviations of the AV angle. We also measured several

331   aspects of cardiac function, including contractility defects that were evident as changes in the

332   diameter of both chambers in diastole and systole (fractional shortening). Unlike other sensitive

333   marine fish species such as bluefin and yellowfin tunas (Incardona et al., 2014), oil exposure did

334   not yield pronounced effects on heart rate or rhythm in red drum. Preliminary assessment of

335   heart rates only showed a significant reduction (bradycardia) at the highest exposure

336   concentrations for the HEWAFs (Fig. S3). Conversely, Slick A and B HEWAFs and LEWAFs

337   all produced a concentration-dependent accumulation of edema (Fig. S4) and chamber looping

338   defects (increased AV angle; Fig. S5). Similarly, the HEWAFs and LEWAFs reduced

339   contractility of atrial and ventricular chambers in a concentration-dependent manner, albeit with

340   a more severe impact on the ventricle (Fig. S6). Notably, the individual chambers showed

15

341 somewhat different responses (Figs. S7 and S8). Oil exposure led to reduction in both the

342 diastolic (relaxed) and systolic (contracted) diameters of the atrium (Fig. S7), but only a

343 reduction in the diastolic diameter of the ventricle (Fig. S8). The reduced diastolic diameters of

344 both chambers are indicative of decreased relaxation of both atrial and ventricular

345 cardiomyocytes. This diastolic dysfunction is consistent with the disruption of sarcoplasmic

346 reticulum-mediated calcium cycling, as previously demonstrated in individual heart muscle cells

347 isolated from tunas and exposed to HEWAF preparations of MC252 crude oil samples (Brette et

348 al., 2014). In particular, this could reflect a failure of the sarcoplasmic reticulum to reuptake

349 calcium through the SERCA2 pump (Louch et al., 2010; Bers, 2014).

350   The reduced systolic diameter was likely caused in part by a reduction in thickness of the

351 atrial cardiac jelly (Fig. S9). Control red drum hearts had a very thick layer of atrial cardiac jelly

352 that was distinctly visible in video frames at peak systole (Fig. S9A). More severely affected oil-

353 exposed hearts generally appeared to have markedly thinner atrial cardiac jelly (Fig. S9B).

354 Although our methods for video collection were not optimized to visualize the cardiac jelly in

355 every animal, we measured thickness in a limited subset of videos in which the myocardial and

356 endocardial boundaries of the jelly were clearly demarcated. Cardiac jelly was reduced at all

357 exposure concentrations, and nonlinear regression showed significant dose-dependency (R^2 =

358 0.89; Fig. S9C). However, an IC_{50} could not be calculated due to a lack of data at even lower

359 exposure concentrations (indicated by the widening 95% confidence interval between the control

360 and lowest tested concentration). This suggests that reduction in cardiac jelly could be an even

361 more sensitive response with a much lower threshold than the other endpoints measured here. A

362 reduction in atrial cardiac jelly was also reported in zebrafish embryos exposed to retene, a C4-

363 alkylated phenanthrene (Scott et al., 2011). More generally, cardiac jelly contributes to the

16

364 intrinsic function of the embryonic heart (Barry, 1948; Baldwin et al., 1994). Thinning of the

365 cardiac jelly could potentially contribute to reduced filling during diastole, or be a compensatory

366 response to myocardial contractile dysfunction resulting from effects on intracellular calcium

367 handling (Brette et al., 2014; Brette et al., 2017).

368 *3.3. Cardiotoxicity thresholds*

369   We used concentration-response modeling to determine the 36-hour IC_{50}/IC_{20} and BMC

370 values for the four different cardiotoxicity endpoints (Fig. 5; Table S4). Thresholds for

371 morphological endpoints (pericardial area and AV angle) were generally higher than those for

372 functional endpoints (atrial and ventricular contractility) for both HEWAF and LEWAF

373 preparations using Slick A or B oil. The HEWAF BMCs for Slick A and B oil generally

374 followed a decreasing trend ranked as pericardial area > AV angle > atrial contractility >

375 ventricular contractility. In addition to being higher, the pericardial area BMCs for both Slick A

376 and B HEWAFs were also more variable than the BMCs for the other three endpoints. However,

377 the LEWAF BMCs for both oils suggested similar toxic thresholds between pericardial area and

378 AV angle, which were both slightly higher than atrial and ventricular contractility thresholds,

379 which were also similar to each other (Fig. 5). This is consistent with observations in other

380 species wherein oil exposure leads to measurable cardiac dysfunction before changes in cardiac

381 morphology, in contrast to the effects of compounds such as dioxins that act through a

382 mechanism strictly dependent on the aryl hydrocarbon receptor (Incardona, 2017).

383   A main goal of this study was to directly compare cardiotoxicity effects levels for WAFs

384 prepared at two very different mixing energies. As HEWAFs contain particulate oil that is

385 potentially less bioavailable (Carls et al., 2008), this comparison was also made using an

386 estimation of dissolved PAH concentrations as described above. The toxicity thresholds (BMCs)

387   for morphological endpoints (pericardial area and AV angle) were higher for Slick A HEWAFs

388   than LEWAFs when based on total TPAH50 measures including both the particulate and

389   dissolved fractions (Fig. 5A, Table S4). The BMCs for the Slick A HEWAF and LEWAF

390   functional endpoints (atrial and ventricular contractility) did not differ significantly, as evidenced

391   by overlapping confidence intervals in Fig. 5A). Based on the estimated dissolved fraction, the

392   effects levels for Slick A HEWAF were more similar to the LEWAF preparations for all

393   endpoints (Fig. 5A, Table S4). For Slick B oil, the toxicity thresholds for the HEWAF were

394   similar to Slick A for all four cardiac endpoints based on total (particulate + dissolved) PAH

395   measures (Fig. 5B, Table S4). For Slick A, the thresholds based on the dissolved fraction of the

396   HEWAFs were lower for all four endpoints. Also, as observed with Slick A, functional

397   cardiotoxicity endpoint thresholds for the LEWAF were similar to those for the estimated

398   dissolved fraction of the HEWAF. However, the two morphological endpoints (pericardial area

399   and AV angle) were relatively less sensitive to Slick B LEWAF. These findings are consistent

400   with the physical properties of the two oil samples (i.e., viscosity and dispersibility) as well as

401   weathering state as a determinant of PAH composition. Toxicity thresholds are generally higher

402   for HEWAFs based on total PAH because non-bioavailable PAHs in particulate oil are included

403   in ∑PAH measures. The very highly weathered Slick B sample was considerably more viscous

404   than Slick A, therefore requiring much higher loadings to yield comparable aqueous PAH

405   concentrations. Moreover, the ratio of more water soluble naphthalenes to less soluble

406   phenanthrenes was higher for Slick B than Slick A (Fig. S1). Thus, based on TPAH measures,

407   Slick B LEWAF would be expected to be less toxic, or have higher thresholds for cardiac injury,

408   than Slick A. While the variance associated with pericardial area (edema accumulation) was

409   higher, metrics for cardiac function were highly and consistently sensitive indicators of toxicity

410   for all exposure categories. These findings are consistent with the known toxicodynamic actions

411   of PAHs; specifically, the role of tricyclic PAHs, and the phenanthrenes in particular, in the

412   disruption of excitation-contraction coupling in cardiomyocytes (Brette at al., 2014, 2017).

413   Importantly, these aspects of cardiotoxicity were virtually indistinguishable between high and

414   low energy WAFs.

415   We did not measure the uptake of PAHs in tissues due to constraints related to very small

416   available sample sizes for fish embryos and larvae. However, numerous previous studies have

417   directly linked tissue PAH levels to embryolarval cardiotoxicity (e.g., (Incardona et al., 2009;

418   Sørensen et al., 2017). Thus, the consistency of the injury endpoints measured here is likely

419   indirect evidence of similar PAH bioavailability to the red drum heart, across the high and low

420   energy exposure preparations. The presence of oil droplets in WAFs influences toxicity largely

421   through changes in toxicokinetics, either as a continuous source of dissolved PAHs (e.g., Carls et

422   al., 2008) or by direct contact (adherence) to the fish egg chorion, thereby providing a higher

423   local concentration to the embryo (e.g., (Sørhus et al., 2015; Sørhus et al., 2016; Sørensen et al.,

424   2017), or both. The former is likely for red drum, as oil droplet binding to the chorion was not

425   observed here or in recent studies of warm-water pelagic spawners such as tunas (Incardona et

426   al., 2014) or mahi mahi (Edmunds et al., 2015).

427   *3.4. Species-specific differences in crude oil toxicity phenotypes*

428   This detailed analysis of cardiotoxicity in red drum also highlights qualitative differences

429   in the crude oil injury phenotype among fish species from the Gulf of Mexico with pelagic

430   embryos and larvae, irrespective of oil exposure preparations in controlled studies. These

431   differences are notable because they likely reflect subtle but important interspecific variation in

432   pathophysiology. The distinctive vulnerability of tunas and amberjack relative to mahi mahi was

19

433   previously attributed to differences in egg size and therefore chemical uptake (Incardona et al.,

434   2014; Edmunds et al., 2015). The individual injury phenotypes observed here for red drum were

435   broader and more severe than previously reported for mahi mahi early life stages (Edmunds et

436   al., 2015; Esbaugh et al., 2016). For red drum, this included a greater degree of edema

437   accumulation and impacts on extracardiac structures such as the head and marginal finfold.

438   However, the overall effects were less severe than those observed for similarly sized tuna

439   embryos (~ 0.9 mm egg). For example, dose-dependent effects on heart rate and rhythm were not

440   observed for red drum as they were for tunas. Although mahi mahi has a significantly larger egg

441   (1.4 – 1.6 mm), this suggests that egg volume is not the sole determinant of toxicity differences

442   among species. This extends our understanding of subtle, species-specific differences in crude oil

443   dysregulation of heart development in fish. As discussed below, the precise nature of the defects

444   we report here are likely a consequence of species differences in life history and ecophysiology.

445   Unlike pelagic, deep-diving tunas (Incardona et al., 2014) and cold-water species such as

446   Pacific herring (Incardona et al., 2009) and Atlantic haddock (Sørhus et al., 2016), crude oil

447   exposures had only a minimal effect on heart rate in red drum, without an induction of

448   arrhythmia. Similar to mahi-mahi and zebrafish, the predominant adverse impact in red drum

449   was reduced contractility and, secondarily, a failure of cardiac looping (all of which lead to a

450   reduction in cardiac output and concomitant accumulation of edema). Contrary to apex predators

451   like the large tunas, red drum is a nearshore/shelf species that resides in relatively shallow water

452   (< 100 m) (Powers et al., 2012) and feeds primarily on benthic invertebrates (Overstreet and

453   Heard, 1978; Scharf and Schlicht, 2000). Although broadly adaptable to gradually changing

454   temperatures, red drum can suffer significant mortality with rapid temperature drops (Saillant et

455   al., 2008). Similarly, the diving behavior of mahi-mahi is limited to shallower and warmer

456   waters (relative to tunas), despite the fast swimming predatory nature of this species (Dagorn et

457   al., 2006; Walli et al., 2009; Merten et al., 2014). Crude oil causes contractility and heart rate and

458   rhythm abnormalities by disrupting cardiomyocyte internal calcium cycling and potassium

459   current-mediated cellular repolarization (i.e., I_{Kr}), respectively (Brette et al., 2014). As further

460   delineated by our findings in red drum, there are two broad classes of responses to oil exposure

461   during cardiac organogenesis: some species respond with both profound bradyarrhythmias (slow,

462   irregular heart beat) plus reduced contractility, while others respond with primarily reduced

463   contractility with minimal effect on heart rate and rhythm. Therefore, we suggest that the

464   aggregate cardiotoxicity phenotype in a given species is likely influenced by the density of the

465   delayed rectifying potassium channels that are necessary for maintaining a steady heart rate at

466   low temperatures. This density is higher in tunas and other species that are tolerant of rapid

467   temperature fluctuations or thrive in extreme cold (Galli et al., 2009; Haverinen and Vornanen,

468   2009) and, thus, they are more susceptible to crude oil-induced impairments of heart rate and

469   rhythm.   This suggests more generally that the severity of functional defects in heart

470   development may follow a gradient of delayed rectifier potassium channel expression levels in

471   cardiomyoctes, in accordance with the ecophysiology of different fish species.

472   *4. Conclusions*

473   Some straightforward conclusions can be drawn from these results. First, in general, HEWAFs

474   generated waterborne PAH profiles that more closely match whole oil, consistent with the

475   presence of entrained oil droplets. In contrast, the profile of LEWAFs were representative of

476   more readily dissolved PAHs - e.g., with parent compounds more abundant than their

477   corresponding alkylated homologs. However, the biological responses of embryos exposed to

478   these two different preparations were virtually indistinguishable, indicating a key role for

479   dissolved PAHs in the injury phenotype. Finally, as observed for other fish species, functional

480   measures of cardiotoxicity were more sensitive than morphological endpoints.

481   **Supporting Information**

482   Tables S1 through S4

483   Figures S1 through S9

484

498

499   **References:**

500   Baldwin, H.S., Lloyd, T.R., Solursh, M., 1994. Hyaluronate degradation affects ventricular

501   function of the early postlooped embryonic rat heart in situ. Circ. Res. 74, 244-252.

502

503   Barry, A., 1948. The functional significance of the cardiac jelly in the tubular heart of the chick

504   embryo. Anat. Rec. 102, 289-298.

505

506   Bers, D.M., 2014. Cardiac sarcoplasmic reticulum calcium leak: basis and roles in cardiac

507   dysfunction. AnnualRreview of Physiology 76, 107-127.

508

509   Brette, F., Machado, B., Cros, C., Incardona, J.P., Scholz, N.L., Block, B.A., 2014. Crude oil

510   impairs cardiac excitation-contraction coupling in fish. Science 343, 772-776.

511

512   Brette, F., Shiels, H.A., Galli, G.L.J., Cros, C., Incardona, J.P., Scholz, N.L., Block, B.A., 2017.

513   A Novel Cardiotoxic Mechanism for a Pervasive Global Pollutant. Sci. Rep. 7, 41476.

514

515   Camilli, R., Reddy, C.M., Yoerger, D.R., Van Mooy, B.A.S., Jakuba, M.V., Kinsey, J.C.,

516   McIntyre, C.P., Sylva, S.P., Maloney, J.V., 2010. Tracking Hydrocarbon Plume Transport and

517   Biodegradation at Deepwater Horizon. Science 330, 201-204.

518

519   Carls, M.G., Holland, L., Larsen, M., Collier, T.K., Scholz, N.L., Incardona, J.P., 2008. Fish

520   embryos are damaged by dissolved PAHs, not oil particles. Aquat. Toxicol. 88, 121-127.

521

522 Dagorn, L., Holland, K.N., Hallier, J.-P., Taquet, M., Moreno, G., Sancho, G., Itano, D.G.,

523 Aumeeruddy, R., Girard, C., Million, J., Fonteneau, A., 2006. Deep diving behavior observed in

524 yellowfin tuna (*Thunnus albacares*). Aquatic Living Resources 19, 85-88.

525

526 Douillet, P.A., Pickering, P.L., 1999. Seawater treatment for larval culture of the fish *Sciaenops*

527 *ocellatus* Linnaeus (red drum). Aquaculture 170, 113-126.

528

529 Dubansky, B., Whitehead, A., Miller, J.T., Rice, C.D., Galvez, F., 2013. Multitissue Molecular,

530 Genomic, and Developmental Effects of the Deepwater Horizon Oil Spill on Resident Gulf

531 Killifish (*Fundulus grandis*). Environ. Sci. Technol. 47, 5074-5082.

532

533 Echols, B.S., Smith, A., Gardinali, P., Rand, G., 2016. An Evaluation of Select Test Variables

534 Potentially Affecting Acute Oil Toxicity. Arch. Environ. Contam. Toxicol. 70, 392-405.

535

536 Edmunds, R.C., Gill, J.A., Baldwin, D.H., Linbo, T.L., French, B.L., Brown, T.L., Esbaugh,

537 A.J., Mager, E.M., Stieglitz, J.D., Hoenig, R., Benetti, D.D., Grosell, M., Scholz, N.L.,

538 Incardona, J.P., 2015. Corresponding morphological and molecular indicators of crude oil

539 toxicity to the developing hearts of mahi mahi. Sci. Rep. 5, 17326.

540

541 Esbaugh, A.J., Mager, E.M., Stieglitz, J.D., Hoenig, R., Linbo, T.L., Lay, C., Forth, H., Brown,

542 T.L., French, B.L., Scholz, N.L., Incardona, J.P., Morris, J.M., Benetti, D.D., Grosell, M., 2016.

543 The effects of weathering and chemical dispersion on Deepwater Horizon crude oil toxicity to

544 mahi-mahi (*Coryphaena hippurus*) early life stages. Sci. Total Environ. 543, 644-651.

545

546 Forth, H.P., Mitchelmore, C.L., Morris, J.M., Lay, C.R., Lipton, J., 2017a. Characterization of

547 dissolved and particulate phases of water accommodated fractions used to conduct aquatic

548 toxicity testing in support of the Deepwater Horizon natural resource damage assessment.

549 Environ. Toxicol. Chem. 36, 1460-1472.

550

551 Forth, H.P., Mitchelmore, C.L., Morris, J.M., Lipton, J., 2017b. Characterization of oil and water

552 accommodated fractions used to conduct aquatic toxicity testing in support of the Deepwater

553 Horizon oil spill natural resource damage assessment. Environ. Toxicol. Chem. 36, 1450-1459.

554

555 Forth, H.P., Morris, J.M., Cacela, D., 2015. Explanation of Analytes Included in the Total

556 Polycyclic Aromatic Hydrocarbon Sums Used by the Deepwater Horizon Natural Resource

557 Damage Assessment Toxicity Group. . National Oceanic and Atmospheric Administration

558 Assessment and Restoration Division.

559

560 Galli, G.L.J., Lipnick, M.S., Block, B.A., 2009. Effect of thermal acclimation on action

561 potentials and sarcolemmal K+ channels from Pacific bluefin tuna cardiomyocytes. Am. J.

562 Physiol. Regul. Integr. Comp. Physiol. 297, R502-R509.

563

564 Haverinen, J., Vornanen, M., 2009. Responses of action potential and K+ currents to temperature

565 acclimation in fish hearts: phylogeny or thermal preferences? Physiol. Biochem. Zool. 82, 468-

566 482.

567

568 Hecht, S.A., Baldwin, D.H., Mebane, C.A., Hawkes, T., Gross, S.J., Scholz, N.L., 2007. An

569 overview of sensory effects on juvenile salmonids exposed to dissolved copper: Applying a

570 benchmark concentration approach to evaluate sublethal neurobehavioral toxicity. NOAA

571 Technical Memorandum NMFS-NWFSC-83. U. S. Dept. of Commerce, p. 39.

572

573 Hicken, C.E., Linbo, T.L., Baldwin, D.H., Willis, M.L., Myers, M.S., Holland, L., Larsen, M.,

574 Stekoll, M.S., Rice, G.S., Collier, T.K., Scholz, N.L., Incardona, J.P., 2011. Sub-lethal exposure

575 to crude oil during embryonic development alters cardiac morphology and reduces aerobic

576 capacity in adult fish. Proc. Natl. Acad. Sci. U. S. A. 108, 7086–7090.

577

578 Holt, J., Godbout, R., Arnold, C.R., 1981. Effects of temperature and salinity on egg hatching

579 and larval survival of red drum, *Sciaenops ocellata*. Fish. Bull. 79, 569-573.

580

581 Incardona, J.P., 2017. Molecular mechanisms of crude oil developmental toxicity in fish. Arch.

582 Environ. Contam. Toxicol. 73, 19-32.

583

584 Incardona, J.P., Carls, M.G., Day, H.L., Sloan, C.A., Bolton, J.L., Collier, T.K., Scholz, N.L.,

585 2009. Cardiac arrhythmia is the primary response of embryonic Pacific herring (*Clupea pallasi*)

586 exposed to crude oil during weathering. Environ. Sci. Technol. 43, 201-207.

587

588 Incardona, J.P., Carls, M.G., Holland, L., Linbo, T.L., Baldwin, D.H., Myers, M.S., Peck, K.A.,

589 Rice, S.D., Scholz, N.L., 2015. Very low embryonic crude oil exposures cause lasting cardiac

590 defects in salmon and herring. Sci. Rep. 5, 13499.

591

592   Incardona, J.P., Gardner, L.D., Linbo, T.L., Brown, T.L., Esbaugh, A.J., Mager, E.M., Stieglitz,

593   J.D., French, B.L., Labenia, J.S., Laetz, C.A., Tagal, M., Sloan, C.A., Elizur, A., Benetti, D.D.,

594   Grosell, M., Block, B.A., Scholz, N.L., 2014. Deepwater Horizon Crude Oil Impacts the

595   Developing Hearts of Large Predatory Pelagic Fish. Proc. Natl. Acad. Sci. U. S. A. 111.

596

597   Incardona, J.P., Scholz, N.L., 2016. The influence of heart developmental anatomy on

598   cardiotoxicity-based adverse outcome pathways in fish. Aquat. Toxicol. 177, 515-525.

599

600   Incardona, J.P., Swarts, T.L., Edmunds, R.C., Linbo, T.L., Edmunds, R.C., Aquilina-Beck, A.,

601   Sloan, C.A., Gardner, L.D., Block, B.A., Scholz, N.L., 2013. Exxon Valdez to Deepwater

602   Horizon: comparable toxicity of both crude oils to fish early life stages. Aquat. Toxicol. 142-143,

603   303-316.

604

605   Jung, J.-H., Hicken, C.E., Boyd, D., Anulacion, B.F., Carls, M.G., Shim, W.J., Incardona, J.P.,

606   2013. Geologically distinct crude oils cause a common cardiotoxicity syndrome in developing

607   zebrafish. Chemosphere 91, 1146-1155.

608

609   Jung, J.H., Kim, M., Yim, U.H., Ha, S.Y., Shim, W.J., Chae, Y.S., Kim, H., Incardona, J.P.,

610   Linbo, T.L., Kwon, J.H., 2015. Differential Toxicokinetics Determines the Sensitivity of Two

611   Marine Embryonic Fish Exposed to Iranian Heavy Crude Oil. Environ. Sci. Technol. 49, 13639-

612   13648.

613

614 Khursigara, A.J., Perrichon, P., Martinez Bautista, N., Burggren, W.W., Esbaugh, A.J., 2017.

615 Cardiac function and survival are affected by crude oil in larval red drum, *Sciaenops ocellatus*.

616 Sci. Total Environ. 579, 797-804.

617

618 Louch, W.E., Hougen, K., Mork, H.K., Swift, F., Aronsen, J.M., Sjaastad, I., Reims, H.M.,

619 Roald, B., Andersson, K.B., Christensen, G., Sejersted, O.M., 2010. Sodium accumulation

620 promotes diastolic dysfunction in end-stage heart failure following Serca2 knockout. J. Physiol.

621 588, 465-478.

622

623 Lowerre-Barbieri, S.K., Burnsed, S.L.W., Bickford, J.W., 2016. Assessing reproductive behavior

624 important to fisheries management: a case study with red drum, Sciaenops ocellatus. Ecol. Appl.

625 26, 979-995.

626

627 Madison, B.N., Hodson, P.V., Langlois, V.S., 2015. Diluted bitumen causes deformities and

628 molecular responses indicative of oxidative stress in Japanese medaka embryos. Aquat. Toxicol.

629 165, 222-230.

630

631 McIntosh, S., King, T., Wu, D., Hodson, P.V., 2010. Toxicity of dispersed weathered crude oil to

632 early life stages of Atlantic herring (*Clupea harengus*). Environ. Toxicol. Chem. 29, 1160-1167.

633

634 Merten, W., Appeldoorn, R., Rivera, R., Hammond, D., 2014. Diel vertical movements of adult

635 male dolphinfish (*Coryphaena hippurus*) in the western central Atlantic as determined by use of

636 pop-up satellite archival transmitters. Mar. Biol. 161, 1823-1834.

637

638 Michel, J., Owens, E.H., Zengel, S., Graham, A., Nixon, Z., Allard, T., Holton, W., Reimer,

639 P.D., Lamarche, A., White, M.M., Rutherford, N., Childs, C., Mauseth, G., Challenger, G.,

640 Taylor, E., 2013. Extent and Degree of Shoreline Oiling: Deepwater Horizon Oil Spill, Gulf of

641 Mexico, USA. PLOS ONE 8, e65087.

642

643 Morris, J.M., M.O. Krasnec, M.W. Carney, H.P. Forth, C.R. Lay, I. Lipton, A.K. McFadden,

644 R. Takeshita, D. Cacela, J.V. Holmes, and J. Lipton. 2015. *Deepwater Horizon* Oil Spill Natural

645 Resource Damage Assessment Comprehensive Toxicity Testing Program: Overview, Methods,

646 and Results. Technical Report. Prepared by Abt Associates, Boulder, CO, for National Oceanic

647 and Atmospheric Administration Assessment and Restoration Division, Seattle, WA. December

648 16. Available in Section 5.12.2 Technical Reports: https://www.fws.gov/doiddata/dwh-ar-

649 documents/952/DWH-AR0293761.pdf

650

651 Mu, J., Jin, F., Ma, X., Lin, Z., Wang, J., 2014. Comparative effects of biological and chemical

652 dispersants on the bioavailability and toxicity of crude oil to early life stages of marine medaka

653 (*Oryzias melastigma*). Environ. Toxicol. Chem. 33, 2576-2583.

654

655 National Research Council, 2011. Guide for the Care and Use of Laboratory Animals, 8th ed.

656 National Academies Press, Washington, D. C.

657

658 Nixon, Z., Zengel, S., Baker, M., Steinhoff, M., Fricano, G., Rouhani, S., Michel, J., 2016.

659 Shoreline oiling from the Deepwater Horizon oil spill. Mar. Pollut. Bull. 107, 170-178.

660   Overstreet, R.M., Heard, R.W., 1978. Food of the red drum, *Sciaenops ocellata*, from

661   Mississippi Sound. Gulf Research Reports 6, 131-135.

662

663   Peterson, C.H., Rice, S.D., Short, J.W., Esler, D., Bodkin, J.L., Ballachey, B.E., Irons, D.B.,

664   2003. Long-term ecosystem response to the Exxon Valdez oil spill. Science 302, 2082-2086.

665

666   Powers, S.P., Hightower, C.L., Drymon, J.M., Johnson, M.W., 2012. Age composition and

667   distribution of red drum (*Sciaenops ocellatus*) in offshore waters of the north central Gulf of

668   Mexico: an evaluation of a stock under a federal harvest moratorium. Fish. Bull. 110, 283-292.

669

670   Saillant, E., Wang, X.X., Ma, L., Gatlin, D.M., Vega, R.R., Gold, J.R., 2008. Genetic effects on

671   tolerance to acute cold stress in red drum, *Sciaenops ocellatus* L. Aquaculture Research 39,

672   1393-1398.

673

674   Sandoval, K., Ding, Y., Gardinali, P., 2017. Characterization and environmental relevance of oil

675   water preparations of fresh and weathered MC-252 Macondo oils used in toxicology testing. Sci.

676   Total Environ. 576, 118-128.

677

678   Scharf, F.S., Schlicht, K.K., 2000. Feeding habits of red drum (Sciaenops ocellatus) in Galveston

679   Bay, Texas: Seasonal diet variation and predator-prey size relationships. Estuaries 23, 128-139.

680

681   Scott, J.A., Incardona, J.P., Pelkki, K., Shepardson, S., Hodson, P.V., 2011. AhR2-mediated;

682   CYP1A-independent cardiovascular toxicity in zebrafish (*Danio rerio*) embryos exposed to

683   retene. Aquat. Toxicol. 101, 165-174.

684

685   Singer, M.M., Aurand, D., Bragin, G.E., Clark, J.R., Coelho, G.M., Sowby, M.L., Tjeerdema,

686   R.S., 2000. Standardization of the preparation and quantitation of water-accommodated fractions

687   of petroleum for toxicity testing. Mar. Pollut. Bull. 40, 1007-1016.

688

689   Sørensen, L., Sørhus, E., Nordtug, T., Incardona, J.P., Linbo, T.L., Giovanetti, L., Karlsen, O.,

690   Meier, S., 2017. Oil droplet binding and differential PAH toxicokinetics in embryos of Atlantic

691   haddock and cod. PLoS One 12, e0180048.

692

693   Sørhus, E., Edvardsen, R.B., Karlsen, O., Nordtug, T., van der Meeren, T., Thorsen, A., Harman,

694   C., Jentoft, S., Meier, S., 2015. Unexpected interaction with dispersed crude oil droplets drives

695   severe toxicity in Atlantic haddock embryos. PLoS One 10, e0124376.

696

697   Sørhus, E., Incardona, J.P., Karlsen, Ø., Linbo, T.L., Sørensen, L., Nordtug, T., van der Meeren,

698   T., Thorsen, A., Thorbjørnsen, M., Jentoft, S., Edvardsen, R.B., Meier, S., 2016. Effects of crude

699   oil on haddock reveal roles for intracellular calcium in craniofacial and cardiac development.

700   Sci. Rep. 6, 31058.

701

702   The Federal Interagency Solutions Group, O.B.C.S.a.E.T., 2010. Oil Budget Calculator -

703   Deepwater Horizon.

704

705   Walli, A., Teo, S.L.H., Boustany, A., Farwell, C.J., Williams, T.D., Dewar, H., Prince, E., Block,

706   B.A., 2009. Seasonal Movements, Aggregations and Diving Behavior of Atlantic Bluefin Tuna

707   (*Thunnus thynnus*) Revealed with Archival Tags. PLoS ONE 4, e6151.

708

709   Xu, E.G., Khursigara, A.J., Magnuson, J., Hazard, E.S., Hardiman, G., Esbaugh, A.J., Roberts,

710   A.P., Schlenk, D., 2017. Larval red drum (*Sciaenops ocellatus*) sublethal exposure to weathered

711   Deepwater Horizon crude oil: developmental and transcriptomic consequences. Environ. Sci.

712   Technol. 51, 10162-10172.

713

714   Ylitalo, G.M., Krahn, M.M., Dickhoff, W.W., Stein, J.E., Walker, C.C., Lassitter, C.L., Garrett,

715   E.S., Desfosse, L.L., Mitchell, K.M., Noble, B.T., Wilson, S., Beck, N.B., Benner, R.A.,

716   Koufopoulos, P.N., Dickey, R.W., 2012. Federal seafood safety response to the Deepwater

717   Horizon oil spill. Proc. Natl. Acad. Sci. U. S. A. 109, 20274-20279.

718

Table 1. TPAH50 exposure concentrations measured at the beginning of each bioassay.

Test	Fraction	Initial TPAH50 Exposure Concentrations (µg/L)					
		Control	A	B	C	D	E
Slick A HEWAF	Total[a]	0.01	1.04	2.61	5.88	9.46	31.53
Slick A HEWAF	Dissolved[b]	0.00	0.55	1.38	2.82	3.03	10.09
Slick B HEWAF	Total	0.05	1.21	3.01	8.71	21.11	51.83
Slick B HEWAF	Dissolved	0.01	0.47	0.97	2.02	3.41	4.88
Slick A LEWAF	Total	0.05	0.96	2.15	4.58	8.97	17.94[c]
Slick B LEWAF	Total	0.01	0.04	0.10	0.40	1.03	14.82

[a]Total PAH sample was not filtered and contains any droplets and dissolved PAHs

[b]Dissolved PAHs estimated according to Forth et al. 2017b

[c]Inferred concentration due to analytical error

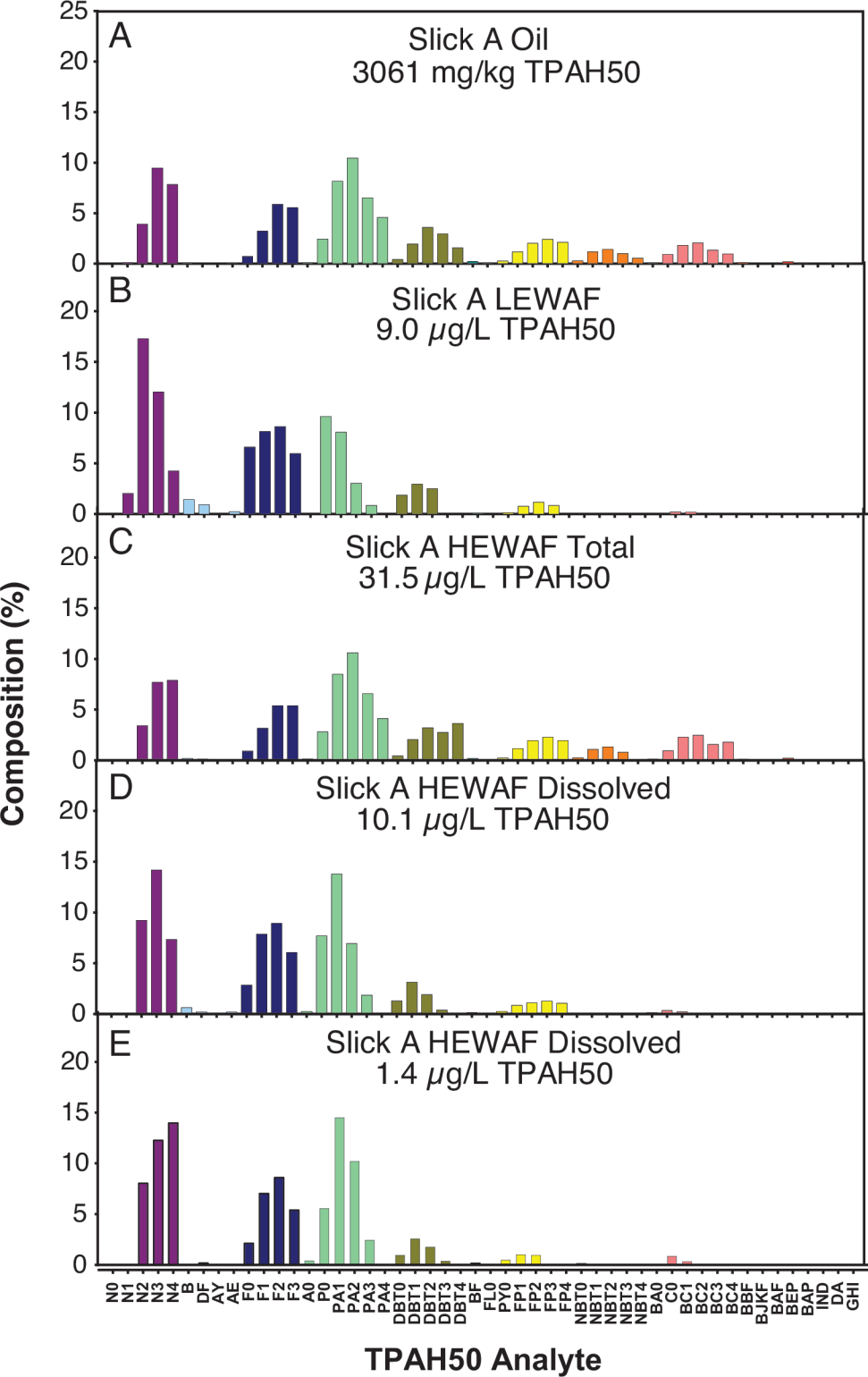719

720   Figure legends

721

722   Figure 1. Percent PAH compositions of Slick A oil and Slick A LEWAF and HEWAF

723   preparations. Dissolved estimates of PAHs for the HEWAF preparations are presented at the low

724   and high exposure concentration ranges based on methods detailed previously(Forth et al.,

725   2017a). The composition is based on the percent of each individual PAH analyte (X-axis labels)

726   compared to the sum of all 50 PAH analytes (TPAH50) listed and defined in Table S1.

727   Figure 2. Percent PAH compositions of Slick B oil and Slick B LEWAF and HEWAF

728   preparations. Dissolved estimates of PAHs for the HEWAF preparations are presented at the low

729   and high exposure concentration ranges based on methods detailed previously(Forth et al.,

730   2017a). The composition is based on the percent of each PAH analyte (X-axis labels) compared

731   to the sum of all 50 PAH analytes (TPAH50) listed and defined in Table S1.

732   Figure 3. Gross morphology of larvae exposed to WAFs through embryogenesis. Representative

733   larvae are shown for control (A) and highest exposure concentration for Slick A (SA) HEWAF

734   (B), Slick B (SB) HEWAF (C), Slick A LEWAF (D), and Slick B LEWAF (E). Representative

735   dorsal views are shown beneath a lateral view for control (A) and Slick B HEWAF (B).

736   Pericardial/yolk sinus edema is indicated by asterisks in all oil-exposed larvae. Arrows indicate

737   eyes in dorsal views (A, B). White arrowheads indicate margins of the dorsal finfold of the head

738   region in lateral views (A – E) and mid-trunk subdermal space in dorsal views (A, B). Scale bar
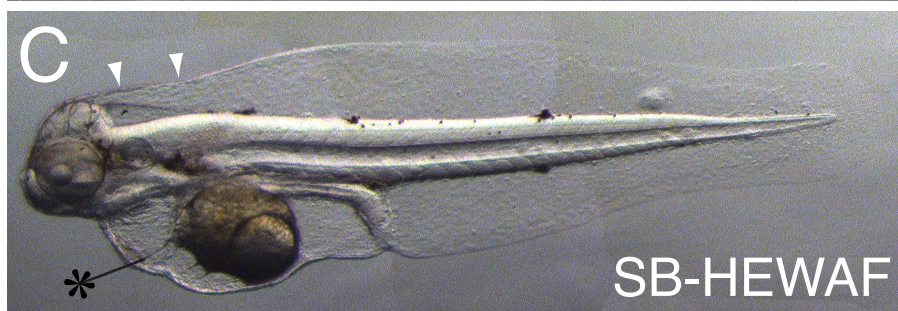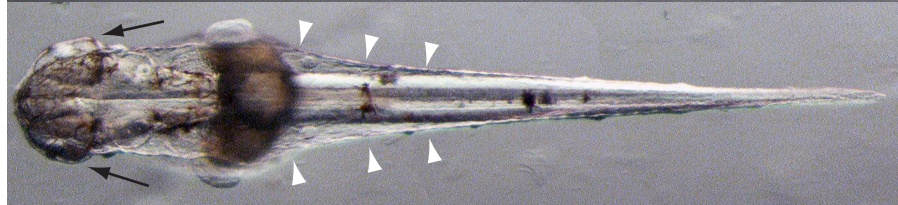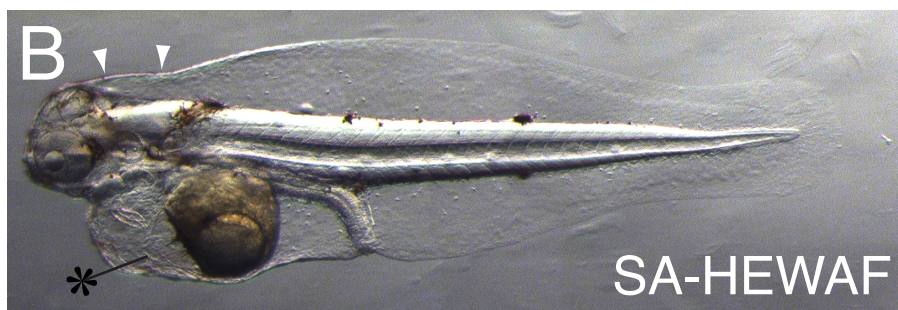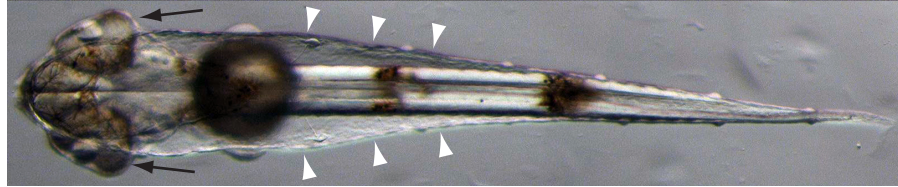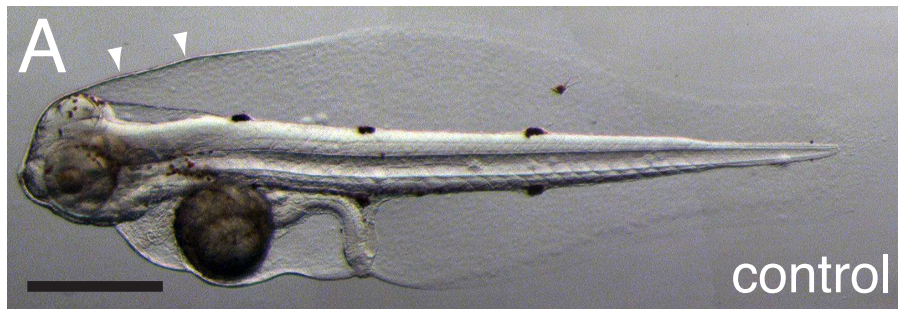
739   is 1 mm.

740   Figure 4. Progressive cardiac malformation in oil-exposed larvae. Ventral view of hatching stage

741   larvae from control (A) and exposed (B) groups. Lateral views of 12 hph larvae from control (C),

742   Slick A HEWAF (D) and Slick B LEWAF (E) exposures. White-filled arrows indicate edema in

743   (B). Black arrowheads without tails demarcate the pericardial/yolk sinus membranes (D, E). *A*,

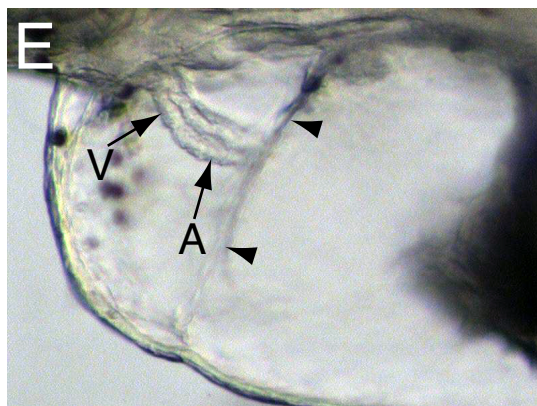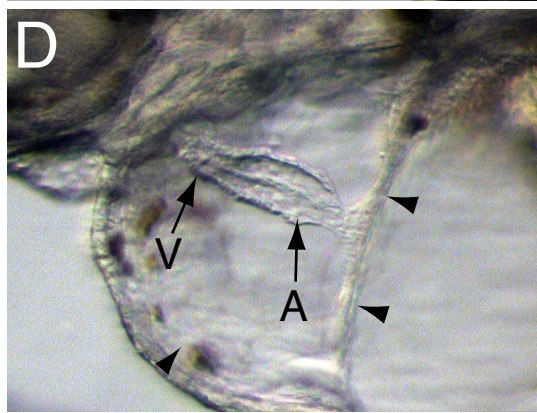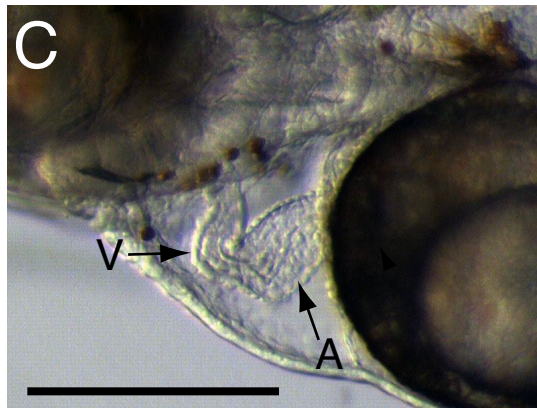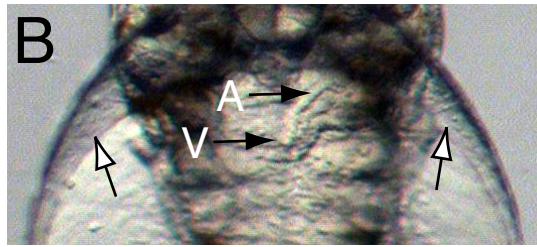744   atrium; *V*, ventricle. Scale bar is 50 µm (A, B; C – E).
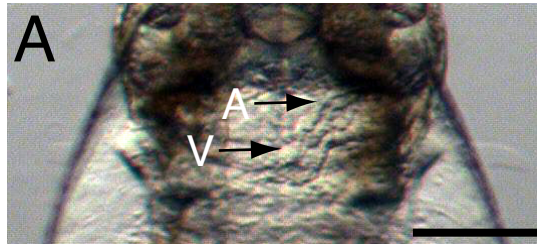
745   Figure 5. 36-hour BMC thresholds for cardio-toxicity endpoints from red drum embryo

746   bioassays with Slick A (panel A) or Slick B (panel B) oil. HEWAF results are presented as

747   measured total and estimated dissolved PAH concentrations. Error bars are 95% confidence

748   intervals.

749

A Slick A Oil
3061 mg/kg TPAH50

B Slick A LEWAF
9.0 μg/L TPAH50

C Slick A HEWAF Total
31.5 μg/L TPAH50

D Slick A HEWAF Dissolved
10.1 μg/L TPAH50

E Slick A HEWAF Dissolved
1.4 μg/L TPAH50

Composition (%)

TPAH50 Analyte

N0 N1 N2 N3 N4 B DF AY AE F0 F1 F2 F3 A0 P0 PA1 PA2 PA3 PA4 DBT0 DBT1 DBT2 DBT3 DBT4 BF FL0 PY0 FP1 FP2 FP3 FP4 NBT0 NBT1 NBT2 NBT3 NBT4 BA0 C0 BC1 BC2 BC3 BC4 BBF BJKF BAF BEP BAP IND DA GHI

Slick B Oil
3257 mg/kg TPAH50

Slick B LEWAF
14.8 μg/L TPAH50

Slick B HEWAF Total
51.8 μg/L TPAH50

Slick B HEWAF Dissolved
4.9 μg/L TPAH50

Slick B HEWAF Dissolved
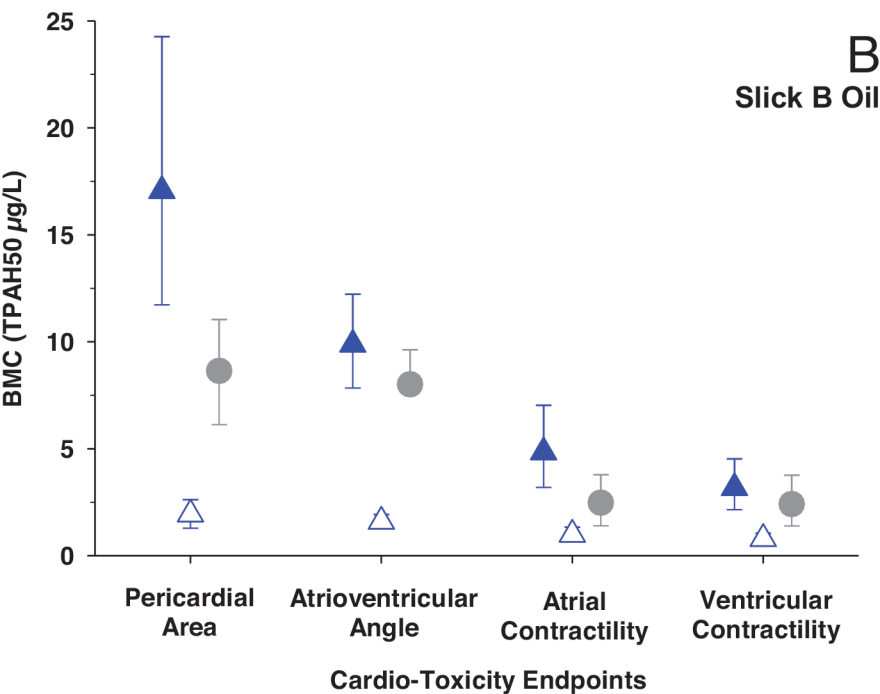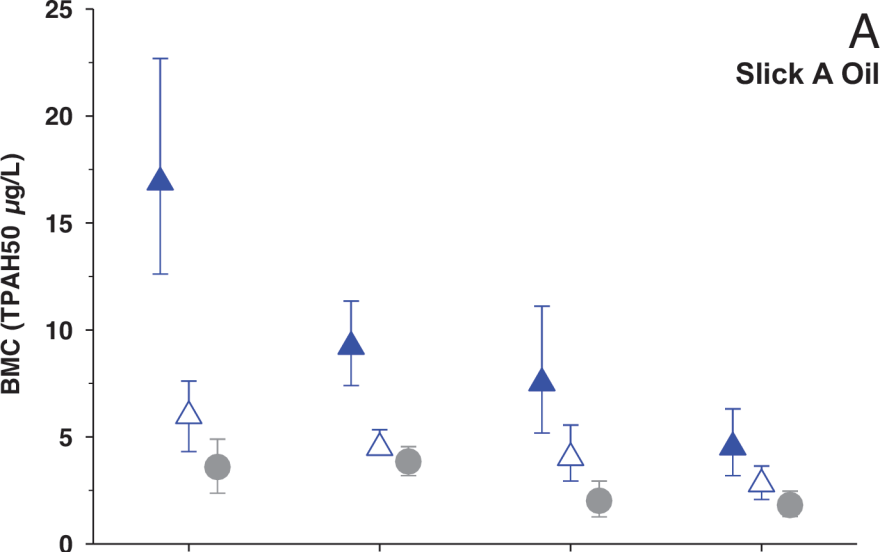0.47 μg/L TPAH50

control

SA-HEWAF

SB-HEWAF

SA-LEWAF

SB-LEWAF

Figure legend:
▲ HEWAF (Total PAH) △ HEWAF (Est. Dissolved PAH) ● LEWAF

Panel A: Slick A Oil
Panel B: Slick B Oil

Y-axis: BMC (TPAH50 μg/L)

X-axis (Cardio-Toxicity Endpoints): Pericardial Area, Atrioventricular Angle, Atrial Contractility, Ventricular Contractility